Theoretical Models of Silica Nanorings: First-Principles Calculations

ARTICLE *in* THE JOURNAL OF PHYSICAL CHEMISTRY C · NOVEMBER 2008

Impact Factor: 4.77 · DOI: 10.1021/jp803668y

THE JOURNAL OF PHYSICAL CHEMISTRY C

Article

Theoretical Models of Silica Nanorings: First-Principles Calculations

Zexiao Xi, Mingwen Zhao, Ruiqin Zhang, Shishen Yan, Tao He, Weifeng Li, Xuejuan Zhang, Xiaohang Lin, Zhenhai Wang, Xiangdong Liu, and Yueyuan Xia

J. Phys. Chem. C, **2008**, 112 (44), 17071-17075• DOI: 10.1021/jp803668y • Publication Date (Web): 14 October 2008

Theoretical Models of Silica Nanorings: First-Principles Calculations

Zexiao Xi,[†] Mingwen Zhao,*[,†] Ruiqin Zhang,[‡] Shishen Yan,[†] Tao He,[†] Weifeng Li,[†] Xuejuan Zhang,[†] Xiaohang Lin,[†] Zhenhai Wang,[†] Xiangdong Liu,[†] and Yueyuan Xia[†]

School of Physics, Shandong University, Jinan 250100, Shandong, P. R. China, and Centre of Super-Diamond and Advanced Films (COSDAF), City University of Hong Kong, Hong Kong SAR, China

Received: April 23, 2008; Revised Manuscript Received: August 15, 2008

We performed first-principles calculations on silica nanorings (NRs) designed via the assembly of two- (2MR), three- (3MR), four- (4MR), and six-membered rings (6MR) in a number of different ways. The stable configurations, energetics, and electronic structures of these NRs are presented. The most stable configurations were found to be size-dependent and to possess different structural features at different size ranges. For small-size silica NRs $(SiO_2)_n$ with $n < 12$, the configurations with 2MR−3MR hybrid structures (2−3MR-NRs) were energetically most stable. For $12 < n < 22$, the NRs formed from linked 2MRs (2MR-NRs) became most favorable. For $n > 22$, the configurations composed of uniformly hybrid 2MRs and 4MRs (2−4MR-NRs) were the most stable structures. The 2−4MR-NRs had the narrowest HOMO−LUMO gaps, which decreased with decreasing n.

I. Introduction

Silica nanoclusters have been the focus of much research over the past few decades, largely due to their important technical applications in nanoelectronics and optics. It has been shown that silica clusters display electronic and optical properties that differ from those of the surface of bulk materials in various experiments, ranging from light adsorption[1] to photoluminescence.[2−4] Understanding the relationship between the structures of silica clusters and their related properties is thus highly desirable.

Silica materials exhibit a diverse spectrum of natural polymorphisms. Recent studies have confirmed the existence of four-, three-, and two-membered rings (4MRs, 3MRs, 2MRs) on the surfaces or interior of amorphous and crystalline silica, as well as vitreous silica. 2MRs can be formed from the condensation of a vicinal hydroxyl group or the thermodynamic rearrangement of the pure silica structure at the surfaces of amorphous and crystalline silica at high temperature.[5−10] Theoretical studies of small-size silica clusters have revealed diverse metastable building blocks with chain,[11,12] ring,[13−15] cage,[16] and tubular[17,18]configurations. The atomic arrangements of these silica clusters formed by assembling 2MRs, 3MRs, and 4MRs differ significantly from the network of silicon-centered corner-sharing SiO_4 tetrahedral of bulk silica, where six-membered rings (6MRs) are found to be the most frequent. The structural features of the silica clusters are related to their high surface-to-bulk ratios that give rise to significant surface reconstruction to reduce the energy.

Among these morphologies, silica nanorings (NRs) are of particular interest because of their unique structural properties and close relationship to silica nanotubes. Bromley et al. proposed $(SiO_2)_n$ NRs resulting from the joining of the end groups of a chain made up of 2MRs.[13] The density functional calculations of $(SiO_2)_n$ chains and rings at the B3LYP/6-311+G(d,p) level show that the rings are energetically more stable than the corresponding linear chains for $n > 11$. Zhao et al. modeled $(SiO_2)_n$ NRs with linked 3MRs of $(SiO_2)_3$ units.[14] First-principles calculations showed that these structures are energetically more favorable at $n = 16$ and 25 than the corresponding linear chains and NRs formed on the basis of 2MRs. Different from the fully coordinated 2MR-NRs, these 3MR-NRs contain nonbridged oxygen atoms (NBOs) terminating the 3MR units. Well-ordered silica nanotubes can be built via assembly of these 3MR-NRs by joining the NBOs to form additional 2MRs.[18] Silica NRs with 2MR−3MR-hybrid structures (2−3MR-NRs) have also been designed from first-principles calculations as energetically favorable building blocks for silica nanocages and layered materials.[15] This enriches the database of silica nanostructures and provides vital information for understanding the growth mechanisms of silica nanomaterials.

The hypothetical nanostructures proposed in theoretical studies offer opportunities for the experimental work that is seeking to realize them. However, the theoretical studies of silica NRs are still limited, and most of the previous work focused on some individual NRs. Searching for more stable configurations of silica NRs composed of 4MRs, 6MRs, or other hybrid units and studying their electronic properties are both highly desirable. To the best of our knowledge, such work has yet to be conducted. To fill this gap, a family of silica NRs was modeled in this work by the assembly of 2MRs, 3MRs, and 2MR−3MR, 2MR−4MR, and 2MR-6MR hybrid units. The stable configurations, energetics, and electronic structures were investigated systematically from first-principles calculations. This work is expected to give theoretical insight into the synthesis and utilization of silica nanomaterials with ringlike or tubular configurations.

II. Methods and Computational Details

We have performed first-principles calculations using an efficient code, SIESTA.[19−21] This is based on density functional theory adopting a localized linear combination of numerical atomic-orbital basis sets for the description of valence electrons and norm-conserving nonlocal pseudopotentials for the atomic core. The pseudopotentials were

* Author to whom correspondence should be addressed. E-mail: zmw@sdu.edu.cn.
† Shandong University.
‡ City University of Hong Kong.

10.1021/jp803668y CCC: $40.75
Published on Web 10/14/2008

constructed using the Trouiller−Martins scheme[22] to describe the valence electron interaction with the atomic core; the nonlocal components of the pseudopotential were expressed in the fully separable form of Kleinman and Bylander.[23,24] The Perdew−Burke−Ernzerhof (PBE) form generalized gradient approximation (GGA) corrections were used for the exchange-correlation potential.[25] The atomic orbital basis set was of double-ζ quality with inclusion of polarization functions (DZP), with a split-norm value for partitioning of the ζ values into inner and outer regions of 0.25. The basis functions were strictly localized within radii that corresponded to a confinement energy of 0.01 Ry, with the exception of the polarization functions, where a fixed radius of 6.0 Bohr was specified. An auxiliary basis set of a real-space grid was used to expand the electron density for numerical integration. A kinetic energy cutoff of 150 Ry was employed to control the fineness of this mesh.

Silica NRs were placed in a supercell with a vacuum region of up to 10 Å along the *x*-, *y*-, and *z*-directions to ensure that isolated NRs were considered. This supercell size was converged in energy calculations within 2 meV/SiO_2 against a size with a vacuum region of 20 Å for these NRs. The equilibrium structures of silica clusters were obtained by relaxing the atomic coordinates with a conjugate gradient (CG) algorithm, reaching a tolerance in the force of $F_{max} < 0.01$ eV/Å. For the silica chains under study, a one-dimensional periodic boundary condition was applied along the *c* axial direction to simulate chains with infinite length, while a vacuum region of up to 10 Å along the direction perpendicular to the *c* axial direction was specified to exclude the mirror interactions. The Brillouin zone of the nanochains was sampled with a *k*-point grid of (1 × 1 × 8), according to the Monkhorst−Pack scheme.[26] To determine the equilibrium structures of silica chains, all the atomic coordinates were optimized using a CG algorithm until the maximal atomic force was below 0.01 eV/Å. The lattice vectors were also optimized simultaneously, with each component of the stress tensor below 0.02 GPa.

III. Results and Discussion

Two main factors, strain and the NBO ratio, affect the stabilization of silica clusters. The strain of silica clusters is mainly dominated by the size and atomic arrangement of *n*MR units. Generally, the larger the *n*MR unit ($n \leq 6$), the lower the strain energy involved in the clusters. NBOs are disadvantageous to the cluster stability because the silicon atoms connected to the NBOs are under-coordinated. Reducing the NBO ratios and increasing the size of the *n*MR units are efficient ways to design more stable configurations of silica clusters. In this work, the 2MR-NRs formed exclusively from 2MRs are free from NBOs, as shown in Figure 1a. The 3MR-NRs composed of linked 3MRs have an NBO ratio of 1/4, as shown in Figure 1b. The 2−3MR-NRs, made up of 2MR-3MR hybrid units, as shown in Figure 1c, have equal numbers of 2MRs and 3MRs and an NBO ratio of 1/6. The 2−4MR-NRs contain equal numbers of 2MRs and 4MRs and exclude NBOs, as shown in Figure 1d. The 2−6MR-NRs have equal numbers of 2MRs and 6MRs and an NBO ratio of 1/4, as shown in Figure 1e. Because of the close relationship between the geometries of NRs and nanochains, we also calculated three silica nanochains formed on the basis of 2MRs (Figure 1f), 2−4MRs (Figure 1g), and 2−6MRs (Figure 1h), respectively. In the present calculations, these nanochains are of infinite length. Both the 2MR-chain and 2−3MR-chain are free from NBOs, while the 2−6MR-chain has an NBO ratio of 1/4.

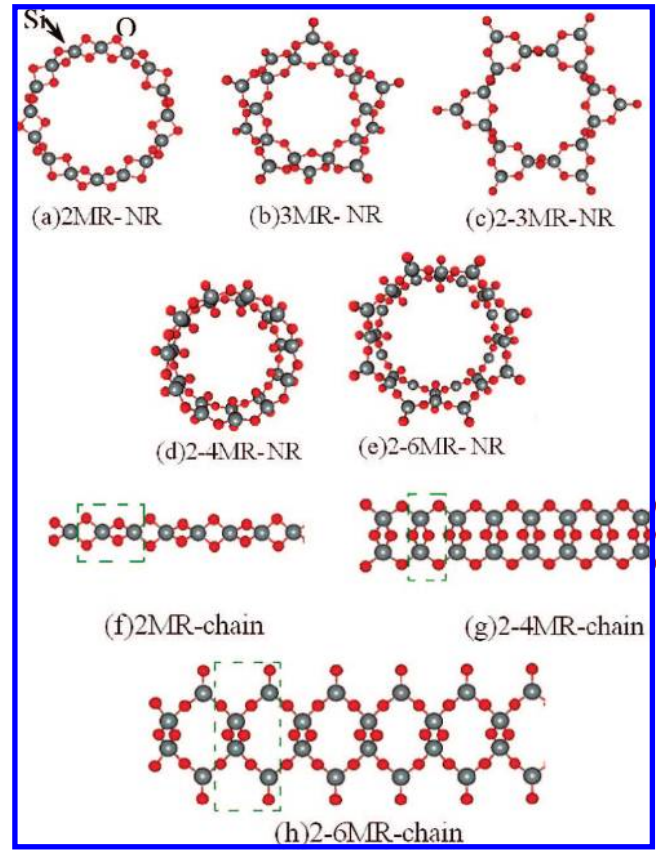

Figure 1. The configurations of the silica NRs and nanochains designed on the basis of 2MR, 3MR, 2−3MR, 2−4MR, and 2−6MR units. Gray balls represent Si atoms, and red balls are O atoms. The dashed rectangles indicate the supercells of the nanochains.

We calculated the energies of these silica NRs $(SiO_2)_n$ and nanochains with respect to that of α-quartz crystal.[27] The evolution of relative energies per SiO_2 unit as a function of the NR sizes, which are represented by *n*, are plotted in Figure 2. With the increase of *n*, the relative energies of 2MR-NRs and 2−4MR-NRs decrease significantly, whereas those of 3MR-NRs, 2−3MR-NRs, and 2−6MR-NRs vary slightly. This is related to the structural features of these NRs. Both 2MR-NRs and 2−4MR-NRs are free from NBOs, and their energies relative to that of α-quartz crystal mainly arise from the curvature-related strain energy of the rings with respect to linear chains and the strain energy inherent in 2MR and 4MR units. The NR size *n* ranges from 6 to 32 in these calculations. The energies of the nanochains are also indicated by the three lines in Figure 2. With the increase of *n* (or the diameter of NRs), the curvature-related strain energy is released rapidly. For the 3MR-NRs, 2−3MR-NRs, and 2−6MR-NRs, however, apart from the strain energies mentioned above, NBOs contribute to the relative energies. Although the strain energies of these NRs are lower than those of 2MR-NRs and 2−4MR-NRs, because 3MR units possess naturally curved configurations and, hence, involve low curvature-related strain energy, NBOs increase the energy remarkably. For each kind of NR, the NBO ratio is constant with increasing size. This leads to a slight variation of the energies of these NRs. It is noteworthy that $(SiO_2)_{18}$ and $(SiO_2)_{20}$ have the lowest energy among 3MR-NRs and 2−3MR-NRs, respectively, as shown in Figure 2b,c. Moreover, the relative energies of 2MR-NRs have an oscillation between the lower *N*-even and the higher *N*-odd ring energy scales, as reported in ref 13, which is related to the mismatch strain. The energy oscillation of 3MR-NRs was also revealed by the present

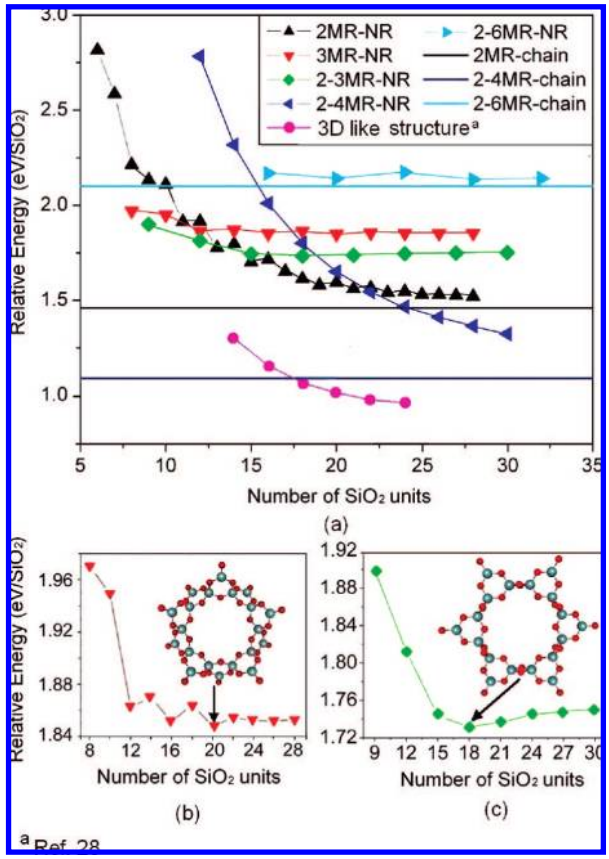

Figure 2. The variation of the relative energy of silica NRs $(SiO_2)_n$ with respect to α-quartz crystal as a function of NR size n. The relative energies of silica nanochains of infinite length are indicated by the lines in this figure. The configurations of the 3D-like clusters were obtained from the ref 28 and optimized in the present calculations.

calculations. The intersections between the variation trends of different kinds of NRs clearly show that the stable configurations of silica NRs are size-dependent. For the NRs with $n < 12$, the structures composed of 2MR-3MR hybrid units are most stable, followed by the structures containing 3MRs, and both of them are energetically more favorable than the NRs of 2MRs. For the NRs with $12 < n < 22$, the 2MR-NRs are the most stable structures, whereas the NRs made up of 2−4MR hybrid units become the most favorable configurations when $n > 22$. The 2−6MR-NRs are the most unstable configurations in the range of sizes under study.

These size-dependent stable configurations are understandable in terms of the compromise of the curvature-related strain energies, the strain energies inherent in nMR units, and the energy increase contributed by NBOs. For small-size NRs, the strain energy of 2MR-NRs is higher than the energy increase of NBOs, and the 2MR-NRs become unstable. The energetic favorability of the 2−3MR-NRs to the 3MR-NRs can be attributed to the low NBO ratio in the 2−3MR-NRs, although the strain energy of the 2−3MR-NRs may be higher than that of the 3MR-NRs because of the high strain energy inherent in 2MR units. With the increasing n, the curvature-related strain energy of the 2MR-NRs is released rapidly, and the 2MR-NRs become the most favorable configurations when $12 < n < 22$. The energetic favorability of the 2−4MR-NRs to the 2MR-NRs when $n > 22$ can be attributed to the lower strain energy inherent in 4MR units compared to that in 2MR units. The 2−6MR-NRs contain highly strained 2MR units and large NBO ratios, and thus have the highest relative energies.

Figure 2 also shows that the 2−4MR nanochain is energetically most favorable, followed by the 2MR nanochain. The 2−6MR nanochain is most unstable. This is related to the structural features of these nanochains. Both the 2−4MR nanochain and the 2MR nanochain are free from NBOs, but the 2−4MR nanochain contains 4MR units whose inherent strain energy is much lower than that of 2MR units. Although the 6MR units of the 2−6MR nanochain have lower inherent strain energy than the 4MR units of the 2−4MR nanochain, they include NBOs with a ratio of 1/4, making the nanochain energetically the most unfavorable among these nanochains. The relative energies of 2MR-NRs and 2−4MR-NRs have a clear tendency to saturate to the values of 2MR and 2−4MR nanochains, respectively, as n is large enough, due to the release of curvature-related strain energies with increasing n. It is noteworthy that when $n > 24$, the 2−4MR-NRs are more stable than the 2MR nanochain, which are the building blocks of the already-synthesized fibrous silica.[29,30] These 2−4MR-NRs, if synthesized, may find potential applications in the construction of novel nanosized silica materials. It should be emphasized that these 2−4MR-NRs cannot form a continuous three-dimensional network via chemical bonds between them because all of the atoms of these 2−4MR-NRs are fully coordinated. However, they can form extended silica polymorphs, such as silica nanotubes, via the possible van der Waals interactions between them,[13] similar to the fibrous silica-w.[29]

In order to address the variation trend of the relative energy of these NRs, we also evaluate the strain energy involved in 2MR and 4MR, relative to α-quartz. For the 2MR and 2−4MR nanochains of infinite length, the contribution of NBOs is excluded; the relative energy of these nanochains with respect to α-quartz can thus be fitted by using the following expressions:

$$\Delta E_1 = \Delta E_{2MR},\ \Delta E_2 = 1/2(\Delta E_{4MR} + \Delta E_{2MR}) \qquad (1)$$

where ΔE_1 and ΔE_2 are the relative energies per SiO_2 unit of 2MR and 2−4MR nanochains, and ΔE_{2MR} and ΔE_{4MR} are the strain energies inherent in 2MR and 4MR. The fitted data from the present calculations are $\Delta E_{2MR} = 1.456$ eV and $\Delta E_{4MR} = 0.732$ eV. The ΔE_{2MR} value agrees well with the result of other ab initio calculations, ∼1.425 eV (±0.055).[31] It is clear that ΔE_{4MR} is much lower than ΔE_{2MR}. That is why the 2−4MR nanochain is more stable than the 2MR nanochain. It is noteworthy that a normal 4MR is expected to have lower strain energy than a 3MR. However, the ΔE_{4MR} value obtained from the present work is larger than that of 3MR (0.21 eV) reported in previous work.[31] This is related to the fact that the 4MR in the 2−4MR nanochains is more strained than a normal 4MR because two of its sides are 2MR rather than larger rings. To minimize such effects of the environment in which a ring is embedded when calculating the strain energy of a n-ring, one normally selects a material with only the n-ring (like the 2MR chain) or only the n-ring and much larger rings (i.e., 6-rings or larger).[31] The contribution of NBO to the relative energy of 3MR-based nanoclusters is estimated to be around 3.555 eV from other ab initio calculations,[14] which is much larger than the figures for 2MR and 2−4MR. This indicates that the silica NRs with large NBO ratios are energetically unfavorable.

The equilibrium structural parameters of 2−4MR-NRs and nanochains are listed in Table 1. From this table, it can be seen that the Si−O bond lengths of NRs are shorter than those of nanochains, and the differences between them decrease with the increase of NR size n. The Si−O bond length elongation of 2−4MR-NRs with respect to that of the 2−4MR nanochain is related to the curvature of the NRs. The 2MR units of the NRs

TABLE 1: Structural Parameters of the 2−4MR-NRs and Nanochains[a]

		Si−O		∠Si−O−Si			
		outer	inner	outer	inner	∠O−Si−O	∠O−Si−Si−O
$(SiO_2)_{12}$	2MR	1.77	1.57	86.2	101.4	86.2	179.8
	4MR	1.74	−	117.4	−	102.6	149.6
$(SiO_2)_{14}$	2MR	1.76	1.59	86.5	97.5	87.9	179.8
	4MR	1.72	−	116.9	−	103.7	152.1
$(SiO_2)_{28}$	2MR	1.70	1.65	88.0	90.9	90.5	179.8
	4MR	1.68	−	114.5	−	110.1	163.6
$(SiO_2)_{30}$	2MR	1.69	1.66	88.1	90.9	90.5	179.6
	4MR	1.68	−	114.4	−	110.8	164.7
2−4MR	2MR	1.68	−	89.0	−	91.0	179.4
	4MR	1.66	−	113.6	−	112.6	180.0
2MR	2MR	1.68	−	88.9	−	91.1	178.9
2−6MR	2MR	1.68	−	87.8	−	91.2	169.9
	6MR	1.64	−	147.9	−	119.3	170.8
α-quartz		1.64		138.8		109.5	−

[a] Distances are in Å and angles are in degrees. "Outer" and "inner" refer to the distance from the NR center.

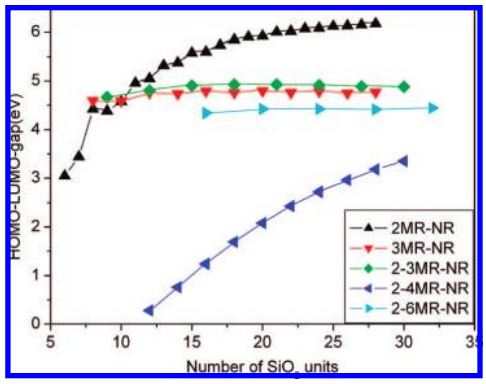

Figure 3. The variation of HOMO−LUMO-gaps of different kinds of NRs as a function of NR size *n*.

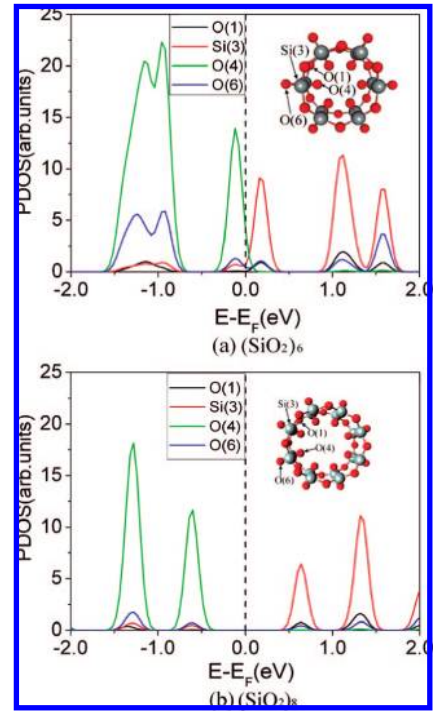

Figure 4. The PDOS of 2−4MR-NRs, $(SiO_2)_{12}$, and $(SiO_2)_{14}$. The energy at Fermi level is set to zero.

are nearly planar. The 2MR and 4MR units are placed alternately. Due to the curvature effects, the inner Si−O−Si angles are larger than the outer Si−O−Si angles, while the inner Si−O lengths are shorter than the outer Si−O lengths.

Additionally, 3D-like structures have been proposed as global minima candidates of silica nanoclusters by Bromley et al.[28] We calculated the energies of five 3D-like silica nanoclusters $(SiO_2)_n$ for n = 14, 16 18, 20, 22, and 24, respectively. These 3D-like structures are energetically more favorable than the ring-like structures proposed in the present work by about 0.6 eV/SiO_2, as shown in Figure 2, implying the metastability of these silica NRs. This is related to the large ratios of NBOs and 2MRs involved in these NRs. However, these silica NRs can act as building blocks to form sheetlike or tubular structures. The assembly of 3MR-NRs via joining the NBOs of one 3MR-NR with the under-coordinated Si atoms of another NR forms silica nanotubes.[18] Silica nanotubes consisting of 2MR and 6MRs can also be built from 2−6MR-NRs through similar method. The $(SiO_2)_{18}$ 2−3MR-NR, which is the energy minima structure of 2−3MR-NRs (shown in Figure 2c), can be regarded as building blocks of silica sheet containing 2MRs embedded by 3MRs.[15,18] The relative energies of silica nanotubes formed from joining 2−6MR-NRs are ∼0.8 eV/SiO_2, while those built from joining 3MR-NRs are only ∼0.6 eV/SiO_2.[18] These silica nanotubes are free from NBOs and subcoordinated Si atoms and thus energetically more advantageous. Another way to avoid the subcoordinated Si atoms is introducing hydroxyls to terminate the clusters. This is related to the instability of silica clusters under aqueous conditions, which is crucial for potential applications in fields ranging from catalysis to drug release. Moreover, the highly strained 2MRs involved in these clusters may be chemically reactive under aqueous conditions. The studies of hydrated silica clusters and the reaction between water molecules and these silica clusters are currently underway in our group and will be reported subsequently.

To enable further understanding of the properties of the molecular rings considered above, we have calculated the electronic structures of all these NRs. The energy gaps, ΔE, between the highest occupied molecular orbital (HOMO) and the lowest unoccupied molecular orbital (LUMO) are plotted in Figure 3. It is interesting to see that, with the increase of n, the energy gaps of 2−4MR-NRs and 2MR-NRs increase substantially, whereas those of other kinds of NRs increase only slightly. The energy gaps of the 2−4MR-NRs are the narrowest among those of all the kinds of NRs under study. We also calculated the electronic energy band structures of the silica nanochains of infinite length and found that the energy band gaps are 9.05, 7.79, and 4.61 eV for the 2MR, 2−6MR, and 2−4MR nanochains, respectively. The band gap of the 2−4MR

nanochain is still the narrowest. Although the Kohn−Sham energy gaps differ from the quasiparticle gaps and are always smaller than the observed values, the energy gap order of these NRs obtained from DFT calculations is reliable.

In order to understand the HOMO−LUMO gap evolution of 2−4MR-NRs, we projected the total electronic density of states (PDOS) of the 2−4MR-NRs with $n = 12$ and 14 onto different atoms, as shown in Figure 4. The HOMO−LUMO gaps are only 0.28 and 0.76 eV for $n = 12$ and 14, respectively. It is obvious that the LUMO arises mainly from the states of Si atoms, while the HOMO arises from the states of interior O atoms. The high strain energy involved in the 2−4MR-NRs with $n = 12$ and 14 increases the energy of HOMO and decreases the energy of LUMO and thus narrows the HOMO−LUMO gaps compared to that of the 2−4MR nanochain. With the increase of the NR size, the curvature-related strain energy is released and the HOMO−LUMO gap increases. Similar curvature-dependent electronic properties have also been reported for silicon carbon nanotubes.[32]

IV. Conclusion

In summary, we have performed first-principles calculations to study the geometric and electronic structures of silica NRs $(SiO_2)_n$ designed via the assembly of 2MR, 3MR, 2−3MR, 2−4MR, and 2−6MR units, respectively. The energetically most favorable configurations are size-dependent. For the NRs with $n < 12$, the 2−3MR-NRs are the most stable configurations. The 2MR-NRs become the most stable structures when $12 < n < 22$. For the large-size NRs with $n > 22$, the 2−4MR-NRs are energetically most favorable. The 2−4MR-NRs have the narrowest HOMO−LUMO gaps, which increase with increasing n.

Acknowledgment. The work described in this paper is supported by the National Natural Science Foundation of China under Grant Nos. 50402017 and 10675075, and the National Basic Research 973 Program of China (Grant No. 2005CB623602). M.W.Z. would like to thank the Program for New Century Excellent Talents for the Universities in China. Another author (R.Q.Z.) would like to thank the support of the Research Grants Council of the Hong Kong Special Administrative Region, China (Project Nos. CityU 103305 and CityU 3/04C).

References and Notes

(1) Altman, I. S.; Lee, D.; Chung, J. D.; Song, J.; Choi, M. *Phys. Rev. B* **2001**, *63*, 161402(R)
(2) Glinka, Y. D. *Phys. Rev. B* **2000**, *62*, 4733.
(3) Glinda, Y. D.; Jaroniec, M. *J. Appl. Phys.* **1997**, *82*, 3499.
(4) Glinda, Y. D.; Lin, S. H.; Chen, Y. T. *Appl. Phys. Lett.* **1999**, *75*, 778.
(5) Ferrari, A. M.; Garrone, E.; Spoto, G.; Ugliengo, P.; Zecchina, A. *Surf. Sci.* **1995**, *323*, 151.
(6) Chiang, C. M.; Zegarski, B. Z.; Dubois, L. H. *J. Phys. Chem.* **1993**, *97*, 6948.
(7) Roder, A.; Kob, W.; Binder, K. *J. Chem. Phys.* **2001**, *114*, 7602.
(8) Bakaev, V. A.; Steele, W. A. *J. Chem. Phys.* **1999**, *111*, 9803.
(9) Ceresoli, D.; Bernasconi, M.; Iarlori, S.; Parrinello, M.; Tosatti, E. *Phys. Rev. Lett.* **2000**, *84*, 3887.
(10) Benoit, M.; Ispas, S. *Phys. Rev. B* **2001**, *64*, 224205.
(11) Nayak, S. K.; Rao, B. K.; Khanna, S. N.; Jena, P. *J. Chem. Phys.* **1998**, *109*, 1245.
(12) Chu, T. S.; Zhang, R. Q.; Cheug, H. F. *J. Phys. Chem. B* **2001**, *105*, 1705.
(13) Bromley, S. T.; Zwijnenburg, M. A.; Maschmeyer, T. *Phys. Rev. Lett.* **2003**, *90*, 035502.
(14) Zhao, M. W.; Zhang, R. Q.; Lee, S. T. *Phys. Rev. B* **2004**, *69*, 153403.
(15) Zhang, D. J.; Zhao, M. W.; Zhang, R. Q. *J. Phys. Chem. B* **2004**, *108*, 48.
(16) de Leeuw, N. H.; Du, Z.; Li, J.; Yip, S.; Zhu, T. *Nano Lett.* **2003**, *3*, 1347.
(17) Zhao, M. W.; Zhang, R. Q.; Lee, S. T. *Phys. Rev. B* **2006**, *73*, 195412.
(18) Zhao, M. W.; Zhu, Z. H.; Gale, J. D.; Xia, Y. Y.; Lu, G. Q. *J. Phys. Chem. C* **2007**, *111*, 9652.
(19) Ordejón, P.; Artacho, E.; Soler, J. M. *Phys. Rev. B* **1996**, *53*, R10441.
(20) Sánchez-Portal, D.; Ordejón, P.; Artacho, E.; Soler, J. M. *Int. J. Quantum Chem.* **1997**, *65*, 453.
(21) Soler, J. M.; Artacho, E.; Gale, J. D.; García, A.; Junquera, J.; Ordejón, P.; Sánchez-Portal, D. *J. Phys.: Condens. Matter.* **2002**, *14*, 2745.
(22) Trouiller, N.; Martins, J. L. *Phys. Rev. B* **1991**, *43*, 1993.
(23) Kleinman, L.; Bylander, D. M. *Phys. Rev. Lett.* **1982**, *48*, 1425.
(24) Bylander, D. M.; Kleinman, L. *Phys. Rev. B* **1990**, *41*, 907.
(25) Perdew, J. P.; Burke, K.; Ernzerhof, M. *Phys. Rev. Lett.* **1996**, *77*, 3865. (b) Perdew, J. P.; Burke, K.; Ernzerhof, M. *Phys. Rev. Lett.* **1997**, *78*, 1396.
(26) Monkhorst, H. J.; Pack, J. D. *Phys. Rev. B* **1976**, *13*, 5188.
(27) The calculations of α-quartz were performed by applying three-dimensional periodical boundary conditions along *x*-, *y*-, and *z*-directions. The Brillouin zone was sampled with a *k*-point grid of $8 \times 8 \times 8$, according to the Monkhorst−Pack scheme. All the atomic coordinates were relaxed until the maximal atomic force was below 0.01 eV/Å. The lattice vectors were also optimized simultaneously, with each component of the stress tensor below 0.02 GPa. The lattice constants obtained from the present calculations are $a = 4.88$ Å and $c = 5.41$ Å, in good agreement with the experimental data, $a = 4.92$ Å and $c = 5.40$ Å.
(28) Bromley, S. T.; Flikkema, E. *Phys. Rev. Lett.* **2005**, *95*, 185505.
(29) Weiss, A.; Weiss, A. *Z. Anorg. Allg. Chem.* **1954**, *276*, 95.
(30) The synthesis of fibrous silica-*w* might be kinetic in nature; i.e., they are formed from joining small silica clusters with 2MR-chain structures in gas phase that lie lowest in energy. In this case, the 2−4MR-NRs lie lower in energy and have no predictive power regarding their synthetic feasibility.
(31) Bromley, S. T.; Moreira, I. P.R.; Illas, F.; Wojdel, J. C. *Phys. Rev. B* **2006**, *73*, 134202.
(32) Zhao, M. W.; Xia, Y. Y.; Li, F.; Zhang, R. Q.; Lee, S. T. *Phys. Rev. B* **2005**, *71*, 085312.

JP803668Y